Hindawi
International Journal of Aerospace Engineering
Volume 2017, Article ID 3812397, 12 pages
https://doi.org/10.1155/2017/3812397

Research Article

The Coupled Orbit-Attitude Dynamics and Control of Electric Sail in Displaced Solar Orbits

Mingying Huo,[1] He Liao,[2] Yanfang Liu,[1] and Naiming Qi[1]

[1]*Department of Aerospace Engineering, Harbin Institute of Technology, Harbin 150001, China*
[2]*Shanghai Satellite Engineering Research Institute, Shanghai 200240, China*

Correspondence should be addressed to Mingying Huo; huomingying123@gmail.com

Received 22 March 2017; Revised 24 May 2017; Accepted 2 July 2017; Published 31 July 2017

Academic Editor: Christian Circi

Displaced solar orbits for spacecraft propelled by electric sails are investigated. Since the propulsive thrust is induced by the sail attitude, the orbital and attitude dynamics of electric-sail-based spacecraft are coupled and required to be investigated together. However, the coupled dynamics and control of electric sails have not been discussed in most published literatures. In this paper, the equilibrium point of the coupled dynamical system in displaced orbit is obtained, and its stability is analyzed through a linearization. The results of stability analysis show that only some of the orbits are marginally stable. For unstable displaced orbits, linear quadratic regulator is employed to control the coupled attitude-orbit system. Numerical simulations show that the proposed strategy can control the coupled system and a small torque can stabilize both the attitude and orbit. In order to generate the control force and torque, the voltage distribution problem is studied in an optimal framework. The numerical results show that the control force and torque of electric sail can be realized by adjusting the voltage distribution of charged tethers.

1. Introduction

Displaced solar orbit is a kind of non-Keplerian orbits, which is lifted above the ecliptic plane by applying a continuous thrust to counterbalance the gravity. From displaced orbit, one would have a continuous view to the polar region of the sun, or a long time scale uninterrupted helioseismological coverage [1]. As a result of that the maintenance of displaced orbit requires continuous propulsive thrust; this mission is impossible for most of conventional (either chemical or electrical) propulsion systems. The solar sail is firstly proposed to maintain the displaced orbits as it utilizes solar radiation pressure to generate continuous and propellant-less thrust. As early as 1929, Oberth mentioned that the solar radiation pressure can be used to generate a displacement between the orbital plane and the ecliptic plane. More recently, large families of displaced solar sail orbits are proposed by McInnes and Simmons [2–4]. The dynamics, stability, and control of displaced solar sail orbits were investigated by considering a solar sail in a rotating frame. Gong et al. did a lot of work on the coupled attitude-orbit dynamics and control of a solar sail in displaced orbits [5, 6] and proposed the solar sail formation flying around displaced orbits [7–10].

However, the thrust acceleration level of solar sails cannot meet the requirements of maintaining high displacement orbits, because its reflection film is not light enough [11]. In addition, as the thrust acceleration of solar sail cannot be adjusted at will between zero and some maximum, the displaced orbit maintained by solar sail is not flexible enough. In light of these problems, the electric solar wind sail (electric sail for short) is used, as an alternative to the use of solar sail, to maintain displaced orbits in this paper. The electric sail, which is first proposed by Janhunen [12] in 2004, is an innovative concept for spacecraft propulsion. Similar to solar sails, electric sails can produce continuous thrust without the need of propellant. Unlike solar sails, electric sails are propelled by the solar wind dynamic pressure, instead of the solar photon momentum.

As shown in Figure 1, the electric sail consists of many tethers, which are held at a high positive potential by a solar-powered electron gun. The electrostatic field generated by the charged tethers can reflect the solar wind protons to

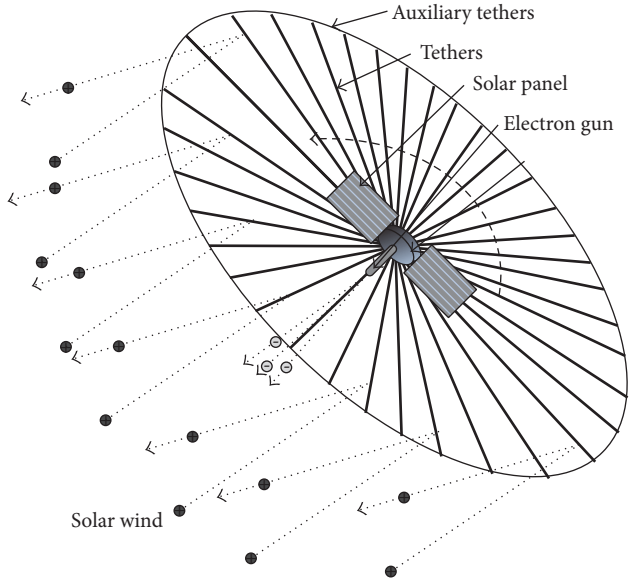

Figure 1: Conceptual sketch of an electric sail.

generate a continuous thrust without any propellant. The deployment and maintenance of electric sail are implemented by spinning the sailcraft about the symmetry axis. It is noticed that an electrostatic field potential structure with a spatial scale larger than 100 m can be created around a thin tether with thickness of a few tens of micrometers. Therefore, the characteristic acceleration of electric sails can be higher than that of solar sails. Recent results show that electric sails can generate 1 N thrust with only 100 kg propulsion system mass [13]. In addition, the thrust of electric sail can be adjusted at will between zero and some maximum by controlling the power of the electron gun [1]. Consequently, the displaced orbit maintained by electric sail is more flexible than that maintained by solar sail. The displaced non-Keplerian orbits for electric sails have been studied by Mengali and Quarta [14]. In their paper, the electric sail capabilities of generating a class of displaced non-Keplerian orbits are analyzed, and a comparison with a solar sail is made. Qi et al. [15] investigated displaced electric sail orbits and the transition trajectory optimization. However, in the above literatures, the displaced orbits of electric sail are researched based on a classical thrust model, and the coupled orbit-attitude dynamics and control of electric sail are not considered. In the classical thrust model, the effects of electric sail attitude on the propulsive thrust modulus and direction were neglected. The thrust modulus was assumed to be invariable with the change of pitch angle, and the thrust cone angle was assumed to be approximately equal to one-half of the pitch angle. Obviously, the above models are not accurate enough to describe the thrust vector of an electric sail for mission analysis. In this paper, the coupled orbit-attitude dynamics and control of electric sail will be considered together based on an advanced thrust model.

Since the propulsive thrust is induced by the sail attitude, the orbital and attitude dynamics of electric-sail-based spacecraft are coupled. However, the coupled orbit-attitude control of electric sails has not been discussed in most published

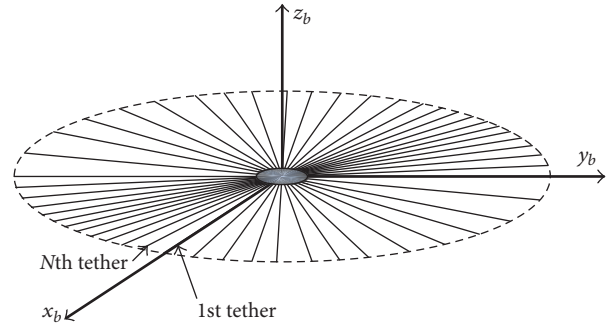

Figure 2: Body reference frame.

literatures. In our previous research [16], the propulsive thrust of electric sail is described as a function of the orbital radius and the sail angle. Consequently, the coupled attitude-orbit dynamics of an electric-sail-based spacecraft are obtained. For the heliocentric transfer mission, the flight control is investigated, wherein the orbital control is studied in an optimal framework via a hybrid optimization method and the attitude controller is designed based on feedback linearization control. In fact, the above attitude and orbital control are carried out separately. Differently, in this paper, the attitude and orbital control of electric sail in displaced solar orbits will be investigated together, instead of being implanted separately.

This paper is organized as follows. First of all, the coupled orbit-attitude dynamics of electric sail are discussed in the heliocentric-ecliptic inertial frame and the body frame. Secondly, the equilibrium point of the coupled dynamical system in displaced orbit is obtained, and its stability is analyzed through a linearization. Finally, the linear quadratic regulator is employed to control the coupled orbit-attitude system for unstable displaced orbits.

2. Coupled Orbit-Attitude Dynamics of Electric Sail

In our previous research [16], the coupled orbit-attitude dynamics of electric sail are obtained. For displaced orbits design and coupled control of electric sail, the coupled dynamics are discussed briefly in this paper.

2.1. Reference Frame. Before the description of coupled dynamics, three reference frames are introduced, which are the body frame $o_b x_b y_b z_b$, the orbital frame $o_o x_o y_o z_o$, and the heliocentric-ecliptic inertial frame $o_i x_i y_i z_i$. Considering an electric sail consists of N tethers as seen in Figure 2, these tethers can be numbered counterclockwise. The origin of the body frame $o_b x_b y_b z_b$ is at the center of mass of the sail, and the x_b-axis is in the direction of a given reference tether. The z_b-axis is along the normal of the sail, and the y_b-axis forms a right-handed system.

The orbital frame $o_o x_o y_o z_o$ and the inertial frame $o_i x_i y_i z_i$ are shown in Figure 3. The origin of the orbital frame $o_o x_o y_o z_o$ is at the center of mass of the sail and the z_o-axis is along the sun-spacecraft direction. The y_o-axis is perpendicular to the

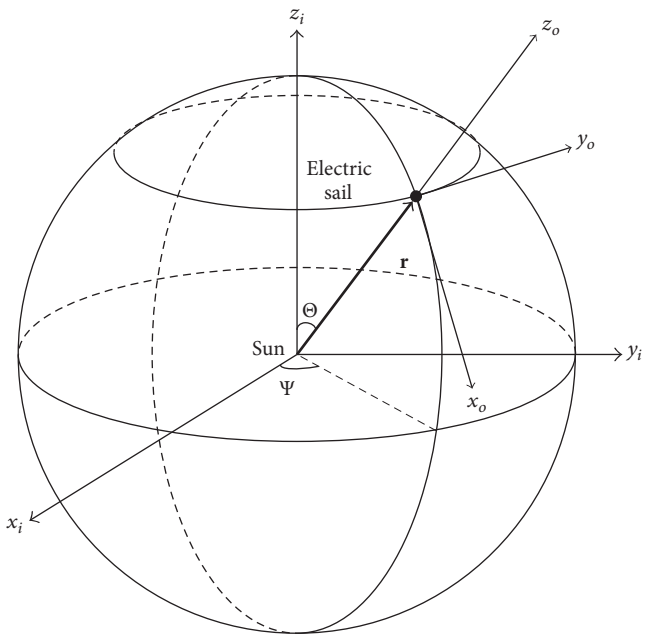

Figure 3: Heliocentric-ecliptic inertial frame and orbital reference frame.

normal of the ecliptic plane and the z_o-axis, and the x_o-axis forms a right-handed triad. The origin of the inertial frame $o_i x_i y_i z_i$ is at the center of mass of the sun, and the x_i-axis is in the direction of sun-equinox. The z_i-axis is along the normal of the ecliptic plane, and the y_i-axis forms a right-handed system. The attitude of the sail in the orbital frame can be described by three angles, ϕ, θ, and ψ, and the rotation sequence from the orbital frame to the body frame is $x(\phi) \rightarrow y(\theta) \rightarrow z(\psi)$.

2.2. Coupled Orbit-Attitude Dynamical Equations. In order to get greater propulsive acceleration and reduce the launch cost, the electric sail must employ large-scale light-weight charged tethers. With these tethers, the electric sail has some special properties of extreme flexibility, low damping, and low frequency. The flexibility of tethers will influence the attitude operation. When the flexible tethers are in motion, the vibration of the structure influences the dynamic characteristics of the entire structure and the coupled control, especially when the structure undergoes large-angle maneuvering. Attitude manoeuvres combined with gyroscopic effects might induce motions that cannot be captured by the rigid body model. However, the coupling mechanism of orbit-attitude-deformation of flexible electric sails is quite complicated. For simplicity, the flexibility of charged tethers is ignored, because the angle of maneuver is small in this paper. As discussed in our previous research [16], the coupled orbit-attitude dynamical scalar equations of electric-sail-based spacecraft, under the assumption of rigid body model, can be written as

$$
\begin{aligned}
\dot{r} &= v_r \\
\dot{\Theta} &= \omega_\Theta \\
\dot{\Psi} &= \omega_\Psi \\
\dot{v}_r &= r\omega_\Psi^2 \sin^2\Theta + r\omega_\Theta^2 - \frac{\mu_\odot}{r^2} \\
&\quad + \frac{\kappa a_\oplus r_\oplus}{2r}\left(\cos^2\phi\cos^2\theta + 1\right) \\
\dot{\omega}_\Theta &= \omega_\Psi^2 \sin\Theta\cos\Theta - \frac{2v_r\omega_\Theta}{r} \\
&\quad + \frac{\kappa a_\oplus r_\oplus}{2r^2}\left(\cos\phi\sin\theta\cos\theta\right) \\
\dot{\omega}_\Psi &= -\frac{2v_r\omega_\Psi}{r} - 2\omega_\Theta\omega_\Psi\cot\Theta \\
&\quad - \frac{\kappa a_\oplus r_\oplus}{2r^2}\left(\sin\phi\cos\phi\cos^2\theta\right) \\
\dot{\phi} &= \frac{\omega_{bx}\cos\psi}{\cos\theta} - \frac{\omega_{by}\sin\psi}{\cos\theta} + \omega_\Psi\sin\Theta \\
&\quad - \omega_\Theta\sin\phi\tan\theta + \omega_\Psi\cos\Theta\cos\phi\tan\theta \\
\dot{\theta} &= \omega_{bx}\sin\psi + \omega_{by}\cos\psi - \omega_\Theta\cos\phi \\
&\quad - \omega_\Psi\cos\Theta\sin\phi \\
\dot{\psi} &= -\omega_{bx}\tan\theta\cos\psi + \omega_{by}\tan\theta\sin\psi + \omega_{bz} \\
&\quad + \frac{\omega_\Theta\sin\phi}{\cos\theta} - \frac{\omega_\Psi\cos\Theta\cos\phi}{\cos\theta} \\
\dot{\omega}_{bx} &= \frac{\omega_{by}\omega_{bz}\left(I_y - I_z\right)}{I_x} + \frac{T_x}{I_x} \\
\dot{\omega}_{by} &= \frac{\omega_{bx}\omega_{bz}\left(I_z - I_x\right)}{I_y} + \frac{T_y}{I_y} \\
\dot{\omega}_{bz} &= \frac{\omega_{bx}\omega_{by}\left(I_x - I_y\right)}{I_z} + \frac{T_z}{I_z},
\end{aligned}
\tag{1}
$$

where r is the distance between sun and sailcraft, Ψ is the ecliptic longitude and Θ is the ecliptic latitude as shown in Figure 3, $\mu_\odot$ is sun's gravitational parameter, thrust control coefficient $\kappa \in [0, 1]$, as the thrust of the electric sail can be adjusted by the electron gun, $a_\oplus$ is the characteristic acceleration of the electric sail, when the sun-spacecraft distance is $r_\oplus = 1\,\text{au}$ (the characteristic acceleration of the electric sail can be adjusted by the electron gun within certain range, $[\omega_{bx}\ \ \omega_{by}\ \ \omega_{bz}]$ is the vector of angular velocity described in the body frame $o_b x_b y_b z_b$, $[T_x\ \ T_y\ \ T_z]$ is the vector of control torque, which can be generated by adjusting the voltage distribution of charged tethers [16], and the inertia matrix of sailcraft $\mathbf{I} = \text{diag}(I_x, I_y, I_z)$, wherein $I_z = 2I_x = 2I_y = 14.666 \times 10^8\ \text{kgm}^2$ in this paper.

3. Displaced Electric Sail Orbits

3.1. Displaced Orbits in General. Solutions of displaced electric sail orbits can be found by seeking equilibrium solutions

to the two-body problem. Considering the definition of displaced orbits in [2], the orbital radius r, the ecliptic latitude Θ, and the ecliptic longitude angle velocity ω_Ψ should be constant and can be chosen to be some particular fixed value. Therefore, the displaced orbits in general should have the following characteristics:

$$\begin{aligned} r &= r_d \\ \Theta &= \Theta_d \\ \omega_\Psi &= \omega_d \\ \dot{r}_d = \ddot{r}_d &= \dot{\Theta}_d = \ddot{\Theta}_d = \dot{\omega}_d = 0, \end{aligned} \tag{2}$$

where r_d, Θ_d, and ω_d are the selected orbital radius, ecliptic latitude, and ecliptic longitude velocity of displaced orbit, respectively.

Substituting (2) in the orbital dynamical scalar equations (1), the required characteristic acceleration $a_{\oplus d}$ and required attitude angles can be obtained as

$$\begin{aligned} a_{\oplus d} &= \frac{3\mu_\odot - 3r_d^3\omega_d^2\sin^2\Theta_d - \chi}{2r_d r_\oplus} \\ \phi_d &= 0 \\ \sin\theta_d &= \sqrt{\frac{\chi + \mu_\odot^2 + r_d^6\omega_d^4\sin^2\Theta_d\left(3\sin^2\Theta_d - 2\right) - r_d^3\omega_d^2\sin^2\Theta_d\left(\chi + 2\mu_\odot\right)}{2r_d^6\omega_d^4\sin^2\Theta_d - 4r_d^3\omega_d^2\sin^2\Theta_d + 2\mu_\odot^2}}\left(\frac{\mu_\odot + \chi - r_d^3\omega_d^2\sin^2\Theta_d}{2r_d^3\omega_d^2\sin\Theta_d\cos\Theta_d}\right), \end{aligned} \tag{3}$$

where $\chi = \sqrt{r_d^6\omega_d^4\sin^2\Theta_d(9\sin^2\Theta_d - 8) - 2\mu_\odot r_d^3\omega_d^2\sin^2\Theta_d + \mu_\odot^2}$.

As shown in (3), the attitude angle ϕ_d should be equal to zero for keeping the required displaced orbit. It means that the normal of the electric sail should be in the same plane as the position vector $\mathbf{r}$ and the orbital angular velocity vector $\boldsymbol{\omega}$. This requirement is consistent with the requirement for keeping displaced orbit using a solar sail [5]. In addition, through a series of analyses, it is known that the chosen parameters of displaced orbit $(r_d, \Theta_d, \omega_d)$ should meet the following criteria:

$$\begin{aligned} &r_d^6\omega_d^4\sin^2\Theta_d\left(9\sin^2\Theta_d - 8\right) - 2\mu_\odot r_d^3\omega_d^2\sin^2\Theta_d + \mu_\odot^2 \\ &\quad \geq 0. \end{aligned} \tag{4}$$

If the selected parameters cannot meet the requirements in (4), electric sails would not be used in keeping the selected displaced orbit, due to the limitation of the maximum thrust cone angle of the electric sail. As discussed in our previous research [16], the thrust cone angle of the electric sail reaches the maximum value 19.47°, when the light incident angle β is 54.75°.

3.2. Displaced Geostationary Orbits. If the orbital period of displaced orbit is chosen to be consistent with the orbital period of Earth, this kind of displaced orbits is named displaced geostationary orbits. Displaced geostationary orbits have the following characteristics:

$$\omega_d = \sqrt{\frac{\mu_\odot}{r_\oplus^3}}. \tag{5}$$

Substituting (5) in (3), the requirements of displaced geostationary orbits are obtained as follows:

$$\begin{aligned} a_\oplus &= \frac{3\mu_\odot r_\oplus^3 - 3\mu_\odot r_d^3\sin^2\Theta_d - \chi r_\oplus^3}{2r_d r_\oplus^4} \\ \phi_d &= 0 \\ \sin\theta &= \sqrt{\frac{\left(\chi + \mu_\odot^2\right)r_\oplus^6 + \mu_\odot^2 r_d^6\sin^2\Theta_d\left(3\sin^2\Theta_d - 2\right) - \mu_\odot r_d^3 r_\oplus^3\sin^2\Theta_d\left(\chi + 2\mu_\odot\right)}{2\mu_\odot^2 r_d^6\sin^2\Theta_d - 4\mu_\odot r_d^3 r_\oplus^3\sin^2\Theta_d + 2\mu_\odot^2 r_\oplus^6}}\left(\frac{\left(\mu_\odot + \chi\right)r_\oplus^3 - \mu_\odot r_d^3\sin^2\Theta_d}{2\mu_\odot r_d^3\sin\Theta_d\cos\Theta_d}\right), \end{aligned} \tag{6}$$

where $\chi = \sqrt{\mu_\odot^2 r_d^6\sin^2\Theta_d(9\sin^2\Theta_d - 8)/r_\oplus^6 - 2\mu_\odot^2 r_d^3\sin^2\Theta_d/r_\oplus^3 + \mu_\odot^2}$.

According to the previous discussion, the chosen parameters of displaced geostationary orbit (r_d, Θ_d) should meet the following criteria:

$$\frac{\mu_\odot^2 r_d^6\sin^2\Theta_d\left(9\sin^2\Theta_d - 8\right)}{r_\oplus^6} - \frac{2\mu_\odot^2 r_d^3\sin^2\Theta_d}{r_\oplus^3} + \mu_\odot^2 \geq 0. \tag{7}$$

Based on (7), we can obtain the feasible region for the displaced geostationary orbit, which is shown in Figure 4.

Based on (6), the required characteristic acceleration $a_{\oplus d}$ and attitude angle θ_d, for keeping displaced geostationary orbits with different parameters (r_d, Θ_d) in feasible region, are calculated and shown in Figures 5 and 6, respectively. As shown in Figure 5, the required characteristic acceleration $a_{\oplus d}$ increases with the decrease of the sun-sailcraft distance and increases with the increase of $|\Theta_d - 90^\circ|$.

4. Stability Analysis

4.1. Analysis of the Stability. In order to facilitate the analysis of the stability of displaced orbits,let $\mathbf{X}_1 = [r, \Theta, \Psi]^{\mathrm{T}}$, $\mathbf{X}_2 = [v_r, \omega_\Theta, \omega_\Psi]^{\mathrm{T}}$, $\mathbf{X}_3 = [\phi, \theta, \psi]^{\mathrm{T}}$, and $\mathbf{X}_4 = [\omega_{bx}, \omega_{by}, \omega_{bz}]^{\mathrm{T}}$. Then, the coupled orbit-attitude dynamical scalar equations of electric-sail-based spacecraft can be written as

$$\begin{aligned}
\dot{\mathbf{X}}_1 &= \mathbf{X}_2 \\
\dot{\mathbf{X}}_2 &= \Gamma\left(\mathbf{X}_1, \mathbf{X}_2, \mathbf{X}_3\right) \\
\dot{\mathbf{X}}_3 &= \Lambda\left(\mathbf{X}_1, \mathbf{X}_2, \mathbf{X}_3, \mathbf{X}_4\right) \\
\dot{\mathbf{X}}_4 &= \Pi\left(\mathbf{X}_4\right),
\end{aligned} \tag{8}$$

where

$$\Gamma = \begin{Bmatrix} r\omega_\Psi^2 \sin^2\Theta + r\omega_\Theta^2 - \dfrac{\mu_\odot}{r^2} + \dfrac{a_\oplus r_\oplus}{2r}\left(\cos^2\phi\cos^2\theta + 1\right) \\ \omega_\Psi^2 \sin\Theta\cos\Theta - \dfrac{2v_r\omega_\Theta}{r} + \dfrac{a_\oplus r_\oplus}{2r^2}\left(\cos\phi\sin\theta\cos\theta\right) \\ -\dfrac{2v_r\omega_\Psi}{r} - 2\omega_\Theta\omega_\Psi\cot\Theta - \dfrac{a_\oplus r_\oplus}{2r^2}\left(\sin\phi\cos\phi\cos^2\theta\right) \end{Bmatrix}$$

$$\Lambda = \begin{Bmatrix} \dfrac{\omega_{bx}\cos\psi}{\cos\theta} - \dfrac{\omega_{by}\sin\psi}{\cos\theta} + \omega_\Psi\sin\Theta - \omega_\Theta\sin\phi\tan\theta + \omega_\Psi\cos\Theta\cos\phi\tan\theta \\ \omega_{bx}\sin\psi + \omega_{by}\cos\psi - \omega_\Theta\cos\phi - \omega_\Psi\cos\Theta\sin\phi \\ -\omega_{bx}\tan\theta\cos\psi + \omega_{by}\tan\theta\sin\psi + \omega_{bz} + \dfrac{\omega_\Theta\sin\phi}{\cos\theta} - \dfrac{\omega_\Psi\cos\Theta\cos\phi}{\cos\theta} \end{Bmatrix} \tag{9}$$

$$\Pi = \begin{Bmatrix} \dfrac{\omega_{by}\omega_{bz}\left(I_y - I_z\right)}{I_x} \\ \dfrac{\omega_{bx}\omega_{bz}\left(I_z - I_x\right)}{I_y} \\ \dfrac{\omega_{bx}\omega_{by}\left(I_x - I_y\right)}{I_z} \end{Bmatrix}.$$

According to the previous discussion, there are equilibrium points of coupled orbit-attitude system in feasible region. By the linearization of the coupled system at the equilibrium point $\mathbf{X}_{\mathrm{ref}} = [\mathbf{X}_{\mathrm{ref1}}^{\mathrm{T}}, \mathbf{X}_{\mathrm{ref2}}^{\mathrm{T}}, \mathbf{X}_{\mathrm{ref3}}^{\mathrm{T}}, \mathbf{X}_{\mathrm{ref4}}^{\mathrm{T}}]^{\mathrm{T}}$, the variational equations are obtained as

$$\begin{aligned}
\delta\dot{\mathbf{X}}_1 &= \delta\mathbf{X}_2 \\
\delta\dot{\mathbf{X}}_2 &= \left.\frac{\partial\Gamma}{\partial\mathbf{X}_1}\right|_{\substack{\mathbf{X}_1=\mathbf{X}_{\mathrm{ref1}} \\ \mathbf{X}_2=\mathbf{X}_{\mathrm{ref2}} \\ \mathbf{X}_3=\mathbf{X}_{\mathrm{ref3}}}} \delta\mathbf{X}_1 + \left.\frac{\partial\Gamma}{\partial\mathbf{X}_2}\right|_{\substack{\mathbf{X}_1=\mathbf{X}_{\mathrm{ref1}} \\ \mathbf{X}_2=\mathbf{X}_{\mathrm{ref2}} \\ \mathbf{X}_3=\mathbf{X}_{\mathrm{ref3}}}} \delta\mathbf{X}_2 \\
&\quad + \left.\frac{\partial\Gamma}{\partial\mathbf{X}_3}\right|_{\substack{\mathbf{X}_1=\mathbf{X}_{\mathrm{ref1}} \\ \mathbf{X}_2=\mathbf{X}_{\mathrm{ref2}} \\ \mathbf{X}_3=\mathbf{X}_{\mathrm{ref3}}}} \delta\mathbf{X}_3 \\
&= \mathbf{A}_1\delta\mathbf{X}_1 + \mathbf{A}_2\delta\mathbf{X}_2 + \mathbf{A}_3\delta\mathbf{X}_3 \\
\delta\dot{\mathbf{X}}_3 &= \left.\frac{\partial\Lambda}{\partial\mathbf{X}_1}\right|_{\substack{\mathbf{X}_1=\mathbf{X}_{\mathrm{ref1}} \\ \mathbf{X}_2=\mathbf{X}_{\mathrm{ref2}} \\ \mathbf{X}_3=\mathbf{X}_{\mathrm{ref3}} \\ \mathbf{X}_4=\mathbf{X}_{\mathrm{ref4}}}} \delta\mathbf{X}_1 + \left.\frac{\partial\Lambda}{\partial\mathbf{X}_2}\right|_{\substack{\mathbf{X}_1=\mathbf{X}_{\mathrm{ref1}} \\ \mathbf{X}_2=\mathbf{X}_{\mathrm{ref2}} \\ \mathbf{X}_3=\mathbf{X}_{\mathrm{ref3}} \\ \mathbf{X}_4=\mathbf{X}_{\mathrm{ref4}}}} \delta\mathbf{X}_2 \\
&\quad + \left.\frac{\partial\Lambda}{\partial\mathbf{X}_3}\right|_{\substack{\mathbf{X}_1=\mathbf{X}_{\mathrm{ref1}} \\ \mathbf{X}_2=\mathbf{X}_{\mathrm{ref2}} \\ \mathbf{X}_3=\mathbf{X}_{\mathrm{ref3}} \\ \mathbf{X}_4=\mathbf{X}_{\mathrm{ref4}}}} \delta\mathbf{X}_3 + \left.\frac{\partial\Lambda}{\partial\boldsymbol{\omega}}\right|_{\substack{\mathbf{X}_1=\mathbf{X}_{\mathrm{ref1}} \\ \mathbf{X}_2=\mathbf{X}_{\mathrm{ref2}} \\ \mathbf{X}_3=\mathbf{X}_{\mathrm{ref3}} \\ \mathbf{X}_4=\mathbf{X}_{\mathrm{ref4}}}} \delta\mathbf{X}_4 \\
&= \mathbf{A}_4\delta\mathbf{X}_1 + \mathbf{A}_5\delta\mathbf{X}_2 + \mathbf{A}_6\delta\mathbf{X}_3 + \mathbf{A}_7\delta\mathbf{X}_4 \\
\delta\dot{\mathbf{X}}_4 &= \left.\frac{\partial\Pi}{\partial\mathbf{X}_4}\right|_{\mathbf{X}_4=\mathbf{X}_{\mathrm{ref4}}} \delta\mathbf{X}_4 = \mathbf{A}_8\delta\mathbf{X}_4,
\end{aligned} \tag{10}$$

where $\mathbf{A}_i$ $(i = 1, 2, \ldots, 8)$ are 3×3 matrixes.

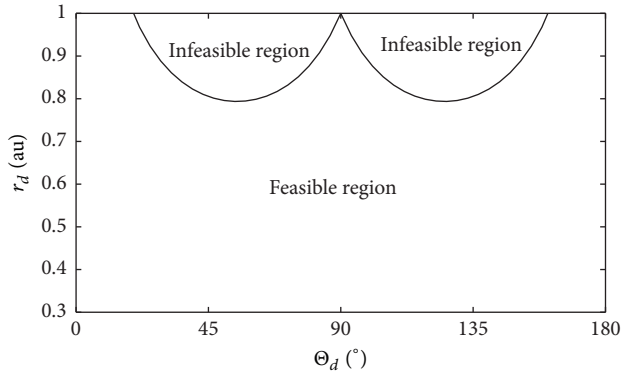

Figure 4: Feasible region for the displaced geostationary orbit.

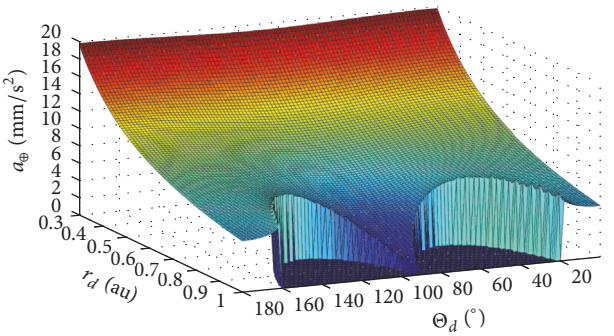

Figure 5: Required characteristic acceleration for the displaced geostationary orbit.

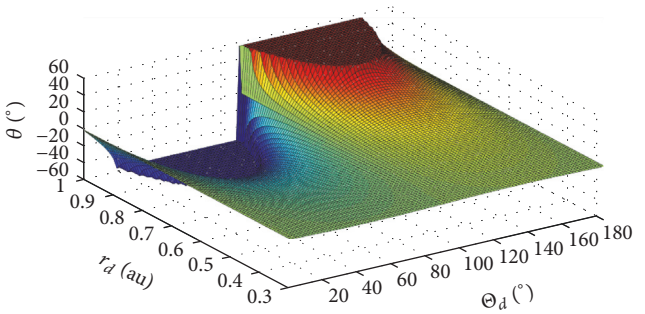

Figure 6: Required attitude angle θ for the displaced geostationary orbit.

Let $\boldsymbol{\delta} = \left[\mathbf{X}_1^{\mathrm{T}} - \mathbf{X}_{\mathrm{ref1}}^{\mathrm{T}} \;\; \mathbf{X}_2^{\mathrm{T}} - \mathbf{X}_{\mathrm{ref2}}^{\mathrm{T}} \;\; \mathbf{X}_3^{\mathrm{T}} - \mathbf{X}_{\mathrm{ref3}}^{\mathrm{T}} \;\; \mathbf{X}_4^{\mathrm{T}} - \mathbf{X}_{\mathrm{ref4}}^{\mathrm{T}}\right]^{\mathrm{T}} = \left[\delta\mathbf{X}_1^{\mathrm{T}} \;\; \delta\mathbf{X}_2^{\mathrm{T}} \;\; \delta\mathbf{X}_3^{\mathrm{T}} \;\; \delta\mathbf{X}_4^{\mathrm{T}}\right]^{\mathrm{T}}$; the variational equations can be written as

$$\dot{\boldsymbol{\delta}} = \begin{bmatrix} 0 & \mathbf{E}_{3\times3} & 0 & 0 \\ \mathbf{A}_1 & \mathbf{A}_2 & \mathbf{A}_3 & 0 \\ \mathbf{A}_4 & \mathbf{A}_5 & \mathbf{A}_6 & \mathbf{A}_7 \\ 0 & 0 & 0 & \mathbf{A}_8 \end{bmatrix} \boldsymbol{\delta} = \mathbf{H}_c \boldsymbol{\delta}, \tag{11}$$

where $\mathbf{E}_{3\times3}$ is a 3×3 identity matrix.

The stability of the equilibrium point can be checked by calculating the eigenvalues of the variational coefficient matrix of coupled system $\mathbf{H}_c$. To quantify the stability of the coupled system, a parameter labeled as characteristic index is defined as the maximal real part of all eigenvalues, given by

$$\Xi_c = \max_{1\le i\le 12} \mathrm{Re}\left(\lambda_i\right), \tag{12}$$

where λ_i $(i = 1, 2, \ldots, 12)$ are eigenvalues of matrix $\mathbf{H}_c$.

According to Lyapunov's stability theory, if $\Xi_c < 0$, the coupled system is asymptotically stable. If $\Xi_c = 0$, the coupled system is marginally stable. If $\Xi_c > 0$, the coupled system is unstable. Referring to (11), the orbital variational coefficient matrix $\mathbf{H}_o$ and the attitude variational coefficient matrix $\mathbf{H}_a$ can be written as

$$\begin{aligned} \mathbf{H}_o &= \begin{bmatrix} 0 & \mathbf{E} \\ \mathbf{A}_1 & \mathbf{A}_2 \end{bmatrix} \\ \mathbf{H}_a &= \begin{bmatrix} \mathbf{A}_6 & \mathbf{A}_7 \\ 0 & \mathbf{A}_8 \end{bmatrix}. \end{aligned} \tag{13}$$

We can also define the characteristic index of orbit and attitude as

$$\begin{aligned} \Xi_o &= \max_{1\le i\le 6} \mathrm{Re}\left(\lambda_{oi}\right) \\ \Xi_a &= \max_{1\le i\le 6} \mathrm{Re}\left(\lambda_{ai}\right), \end{aligned} \tag{14}$$

where λ_{oi} $(i = 1, 2, \ldots, 6)$ are eigenvalues of the orbital variational coefficient matrix $\mathbf{H}_o$ and λ_{ai} $(i = 1, 2, \ldots, 6)$ are eigenvalues of the attitude variational coefficient matrix $\mathbf{H}_a$.

4.2. Numerical Analysis of the Stability. In this section, the linearized coupled dynamical equations are employed to investigate the stability of the coupled equilibrium numerically. An arbitrary displaced orbit is selected to investigate the relation between the stability of the coupled system and the parameter ω_d. The selected displaced orbit for simulation is determined by $r_d = 0.9$ au and $\Theta_d = 86^\circ$. The range of selected orbital angular velocity for simulation is $\omega_d \in [0.5\omega_\oplus, 5\omega_\oplus]$. Other displaced orbits can be analyzed in the same way. As shown in Figure 7, it is found that the orbital system of selected displaced orbit is unstable when the selected orbital angular velocity ω_d is less than a critical value (the critical value is $0.84\omega_\oplus$ for $r_d = 0.9$ au and $\Theta_d = 86^\circ$). It is marginally stable when the selected orbital angular velocity ω_d is more than the critical value. Figure 8 indicates that the attitude system is always marginally stable and ω_d does not influence the stability.

Figure 9 indicates that the coupled system of selected displaced orbit is unstable when the selected orbital angular velocity ω_d is less than a critical value (the critical value is $1.32\omega_\oplus$ in this simulation). The coupled system is marginally stable when the selected orbital angular velocity ω_d is more than the critical value. Therefore, it is easy to be known that the displaced geostationary orbit ($\omega_d = \omega_\oplus$) with $r_d = 0.9$ au and $\Theta_d = 86^\circ$ is unstable for a fixed attitude.

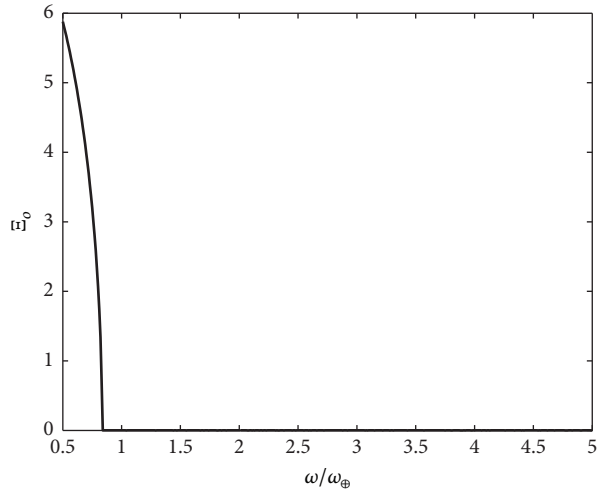

Figure 7: Orbital characteristic index Ξ_o as a function of the angular velocity ω_d.

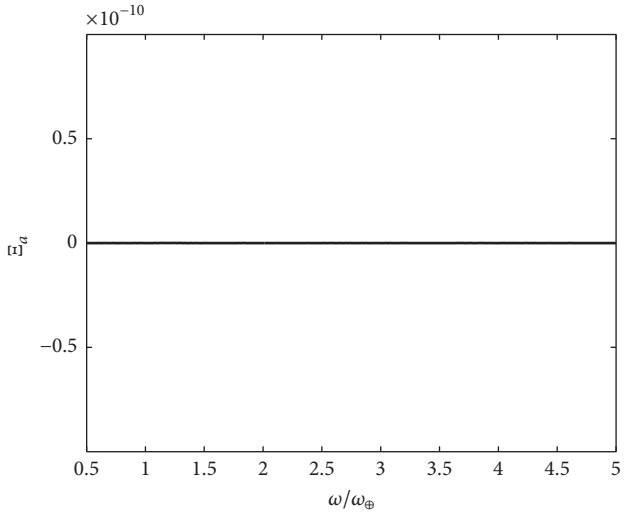

Figure 8: Attitude characteristic index Ξ_a as a function of the angular velocity ω_d.

5. Coupled Orbit-Attitude Control of Electric Sail

5.1. Control Algorithm. The stability of the displaced orbit has been discussed above. The numerical results show that only some of displaced orbits are marginally stable. Therefore, active control is necessary to stabilize the unstable displaced orbits. In this paper, only control torque is employed to stabilize both the attitude and orbit of sailcraft. Then, the coupled system can be linearized and the corresponding linear system is employed for control design. The coupled equations linearized at the equilibrium point with control torque can be written as

$$\dot{\boldsymbol{\delta}} = \mathbf{H}_c\boldsymbol{\delta} + \mathbf{B}\mathbf{u}, \tag{15}$$

where $\boldsymbol{\delta} = [\delta r, \delta\Theta, \delta\Psi, \delta v_r, \delta\omega_\Theta, \delta\omega_\Psi, \delta\phi, \delta\theta, \delta\psi, \delta\omega_x, \delta\omega_y, \delta\omega_z]^{\mathrm{T}}$ is state perturbation, $\mathbf{H}_c$ is the variational coefficient matrix of coupled system, $\mathbf{B} = [0_{3\times3}, 0_{3\times3}, 0_{3\times3}, 1/\mathbf{I}]^{\mathrm{T}}$ ($\mathbf{I}$ is the inertia matrix of sailcraft), and $\mathbf{u} = \mathbf{T} = [T_x, T_y, T_z]^{\mathrm{T}}$ is the vector of control torque.

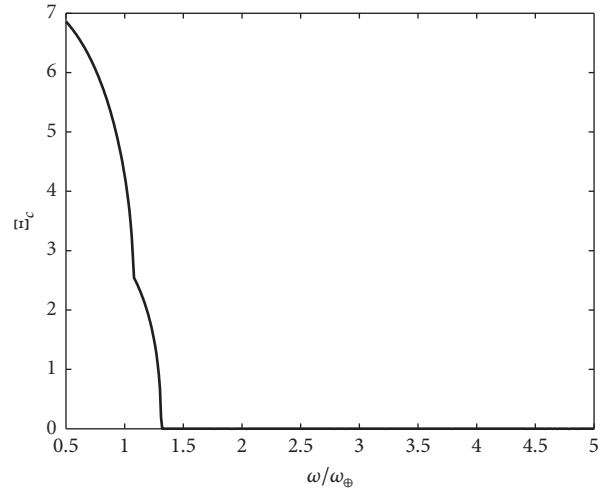

Figure 9: Coupled-system characteristic indexes Ξ_c as a function of the angular velocity ω_d.

In order to determine the controllability of this system, the rank of the controllability matrix of the linearized system has been calculated. The results show that the system is controllable, because the controllability matrix has full rank. In this paper, linear quadratic regulator (LQR) is employed to design the control torque to track the desired attitude and orbit. The performance function is selected as

$$J = \int_0^\infty \left(\boldsymbol{\delta}^{\mathrm{T}}\mathbf{Q}\boldsymbol{\delta} + \mathbf{u}^{\mathrm{T}}\mathbf{R}\mathbf{u}\right) \mathrm{d}t, \tag{16}$$

where the matrix $\mathbf{Q} \in \mathbb{R}^{12\times12}$ is symmetric positive definite and represents the weight of the state errors. The matrix $\mathbf{R} \in \mathbb{R}^{3\times3}$ is also a symmetric positive definite matrix and represents the weight of the control input.

The linear state feedback can be obtained by solving the following algebraic Riccati matrix:

$$\mathbf{P}\mathbf{H}_c + \mathbf{H}_c\mathbf{P} - \mathbf{P}\mathbf{B}\mathbf{R}^{-1}\mathbf{B}^{\mathrm{T}}\mathbf{P} + \mathbf{Q} = 0. \tag{17}$$

Then, the control torque can be written in the state-feedback form as

$$\mathbf{u} = -\mathbf{R}^{-1}\mathbf{B}^{\mathrm{T}}\mathbf{P}\boldsymbol{\delta}. \tag{18}$$

5.2. Numerical Simulation. In order to investigate the stability of the displaced orbit with linear quadratic regulator control, a numerical example is adopted in this section, using the full nonlinear dynamical equations. The selected displaced orbit for simulation is a displaced geostationary orbit ($\omega_d = \omega_\oplus$) and is determined by $r_d = 0.9$ au and $\Theta_d = 86^\circ$. For keeping the selected displaced geostationary orbit, the required characteristic acceleration $a_{\oplus d}$ should be equal to 1.942 mm/s^2, and attitude angle θ_d should be equal to -21.749°. As discussed above, the chosen displaced orbit

is unstable without control. Assume that the orbit and the attitude have a small perturbation to the required orbit and attitude at the initial time. The initial values of the perturbation are given by $\delta\mathbf{X}_1 = [4 \times 10^4\,\mathrm{m}, 0, 0]^{\mathrm{T}}$, $\delta\mathbf{X}_2 = [0, 0, 0]^{\mathrm{T}}$, $\delta\mathbf{X}_3 = [0, 0.2^\circ, 0]^{\mathrm{T}}$, and $\delta\mathbf{X}_4 = [0, 0, 0]^{\mathrm{T}}$. Figures 10 and 11 give the responses of attitude and orbit, respectively. Numerical simulation shows that the LQR control law can control the coupled system. As shown in Figure 12, a small control torque can stabilize both the attitude and orbit.

5.3. Preliminary Study of Voltage Distribution. The control torque of electric sail can be realized by adjusting the voltage distribution of charged tethers of electric sail [16, 17]. In this paper, the generation of control torques is preliminarily discussed in an optimal framework. Referring to Eq. (10) and Eq. (13) in [16], the vector of propulsive force $\mathbf{F}$ and the vector of control torque $\mathbf{T}$ can be written as functions of the vertical thrust magnitude of charged tethers $\sigma_{\oplus 1}, \ldots, \sigma_{\oplus N}$.

$$\begin{aligned}\mathbf{F}\left(\phi, \theta, \psi, r, l, \sigma_{\oplus 1}, \ldots, \sigma_{\oplus N}\right) &= \sum_{k=1}^{N} \mathbf{F}_k\left(\phi, \theta, \psi, r, l, \sigma_{\oplus k}\right)\\ \mathbf{T}\left(\phi, \theta, \psi, r, l, \sigma_{\oplus 1}, \ldots, \sigma_{\oplus N}\right)&\\ = \sum_{k=1}^{N} \mathbf{T}_k\left(\phi, \theta, \psi, r, l, \sigma_{\oplus k}\right),&\end{aligned} \tag{19}$$

where $\sigma_{\oplus k}$, $k \in [1, N]$, is the kth tether's magnitude of the force per unit length, when the sun-spacecraft distance is $r_\oplus = 1$ au and the solar wind is perpendicular to tether. As discussed in [17], $\sigma_{\oplus k}$ can be controlled by altering the voltage of kth charged tether V_k and is given by

$$\sigma_{\oplus k} = 0.18 \max\left(0, V_k - V_0\right) \sqrt{\varepsilon_0 p_{\mathrm{dyn}}}, \tag{20}$$

where V_0 is the electric potential corresponding to the kinetic energy of the solar wind ions, ε_0 is the vacuum permittivity, and p_{dyn} is the solar wind dynamic pressure.

In order to generate the required control force $\mathbf{F}_c$ and control torque $\mathbf{T}_c$, the following equality constraints should be satisfied:

$$\begin{aligned}\sum_{k=1}^{N} \mathbf{F}_k\left(\phi, \theta, \psi, r, l, \sigma_{\oplus k}\right) &= \mathbf{F}_c\\ \sum_{k=1}^{N} \mathbf{T}_k\left(\phi, \theta, \psi, r, l, \sigma_{\oplus k}\right) &= \mathbf{T}_c.\end{aligned} \tag{21}$$

As shown in (21), the quantity of equality constraints is 6 in voltage distribution problem. Comparatively, the number of design variables $\sigma_{\oplus 1}, \ldots, \sigma_{\oplus N}$ is $N \in [20, 100]$ in general, which is decided by the quantity of charged tethers of electric sail. Therefore, the definite solution cannot be obtained by solving (21). In this paper, the voltage distribution problem is converted into a nonlinear programming problem (NLP). Equation (21) is processed into equality constraints in optimal framework. In order to reduce the required power, the optimization performance index is selected as follows:

$$J = \sum_{k=1}^{N} \sigma_{\oplus k}. \tag{22}$$

The above NLP can be solved within the MATLAB environment using *fmincon*, which is a constrained optimization routine available with the Optimization Toolbox. The selected optimization algorithm is sequential quadratic programming (SQP). Consider an electric sail, which is composed of $N = 100$ 20 km-long tether. At the beginning of the mission, the required control force can be calculated according to (1), with the required characteristic acceleration $a_{\oplus d} = 1.942\,\mathrm{mm/s^2}$ and attitude angle $\theta_d = -21.949^\circ$. As seen in Figure 12, the required control torque is $T = [9.3941 \times 10^{-5}, -6.1 \times 10^{-3}, 1.8116 \times 10^{-6}]$ Nm at the beginning of the mission.

This NLP was solved in 2.453 seconds using a personal computer with 8 GB RAM running at 2.20 GHz processor speed. The obtained thrust magnitudes per unit length $\sigma_{\oplus k}$, $k \in [1, N]$, are shown in Figure 13. Considering (20), the required voltage distribution V_k, $k \in [1, N]$, can be obtained and is shown in Figure 14, where $V_{\mathrm{aver}} = \sum_{k=1}^{N} V_k$ is the average value of V_k, $k \in [1, N]$. Through the preliminary study of voltage distribution, it can be found that the control force and torque of electric sail can be realized by adjusting the voltage distribution of charged tethers. This feature is quite different between traditional torque-generated methods, in which the actuator is at the bus center in general.

Even though a solar sail and an electric sail are both capable of producing a propulsive thrust without the need of any propellant, these two propulsion systems are substantially different in terms of performance, shape, and dimensions [18]. Compared to the dynamics and control of solar sail discussed in [6], the difference is mainly reflected in the following aspects. In terms of propulsion mechanism, electric sails are propelled by the solar wind dynamic pressure using charged tethers, instead of the solar photon momentum. In the thrust model of solar sail, the thrust cone angle of ideal solar sail is equal to the pitch angle. Differently, the thrust cone angle of electric sail reaches a maximum value of 19.47°, when pitch angle is equal to 54.75°. This feature causes the fact that there are infeasible regions for the displaced geostationary orbit using electric sail, as shown in Figure 4. About the difference on control, the control force and control torque of electric sail can be realized by adjusting the voltage distribution of charged tethers, as discussed in this section. This feature is quite different from solar sail.

6. Conclusions

In this paper, displaced solar orbits for spacecraft propelled by electric sails are investigated as an alternative to solar sails. Since the propulsive thrust is induced by the sail attitude, the orbital and attitude dynamics of electric-sail-based spacecraft are coupled and investigated together. The equilibrium

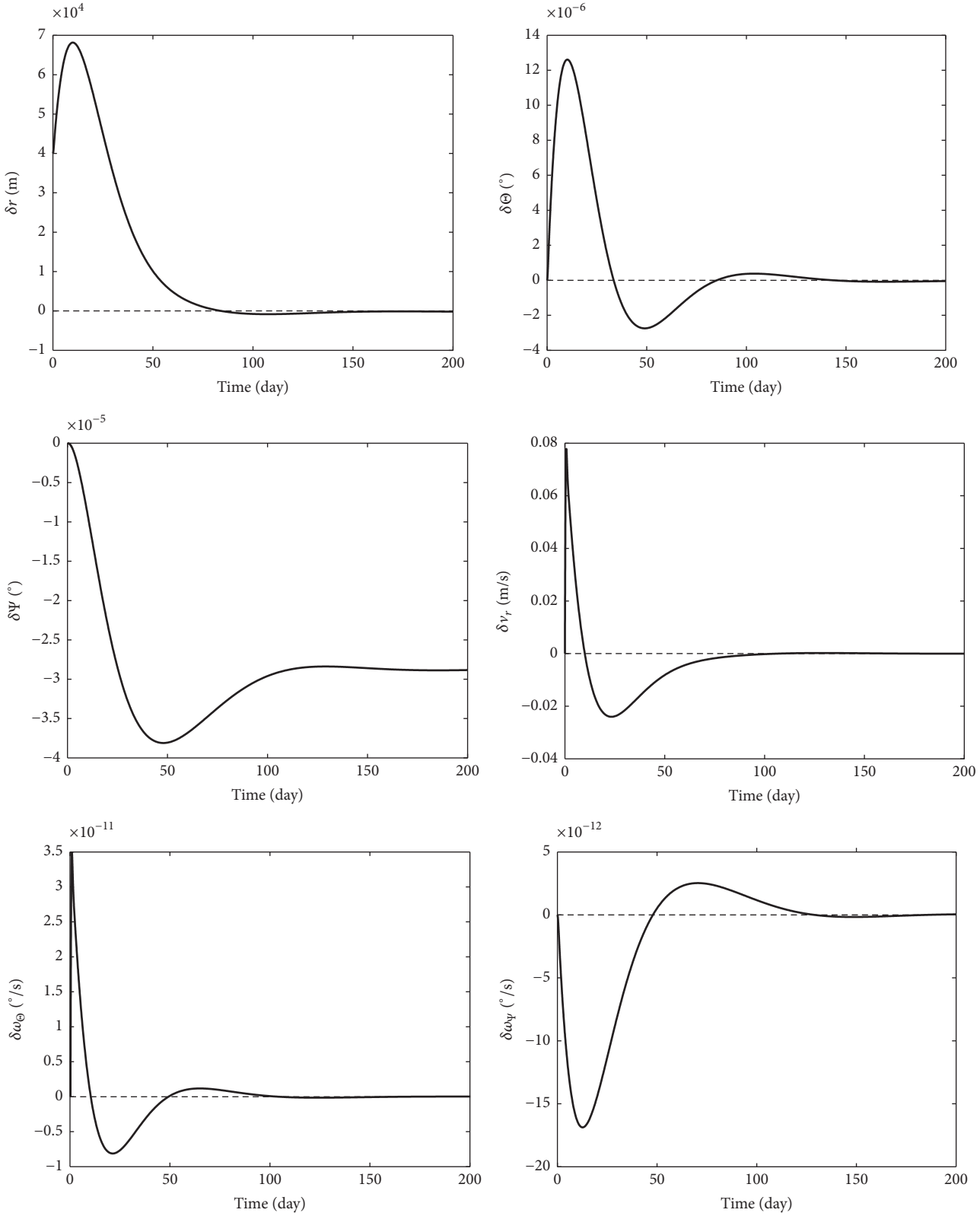

Figure 10: The responses of the orbit errors.

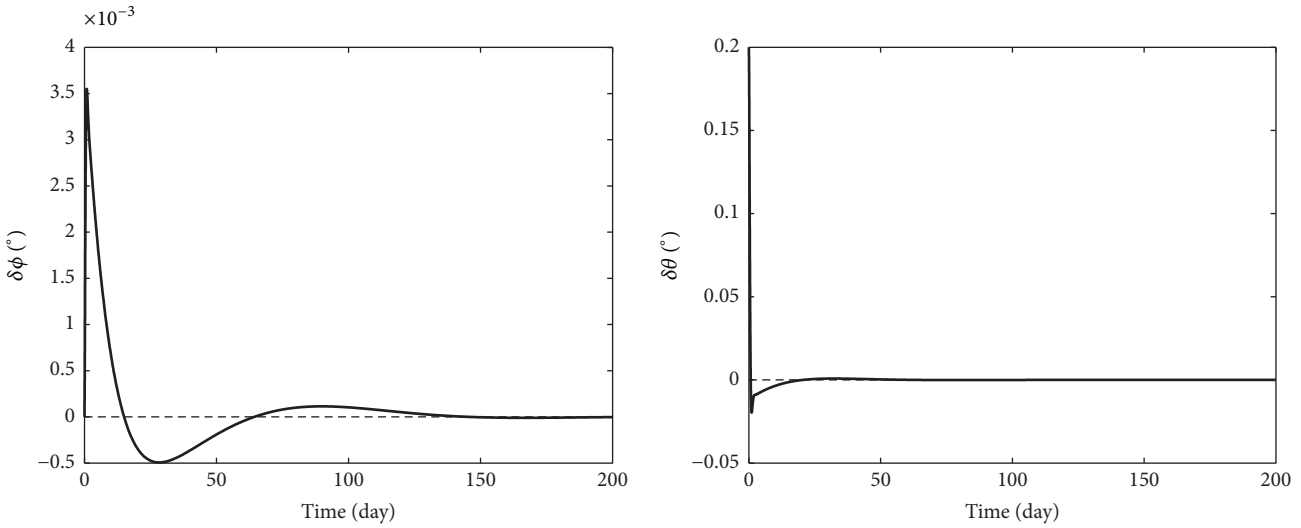

Figure 11: The responses of the attitude errors.

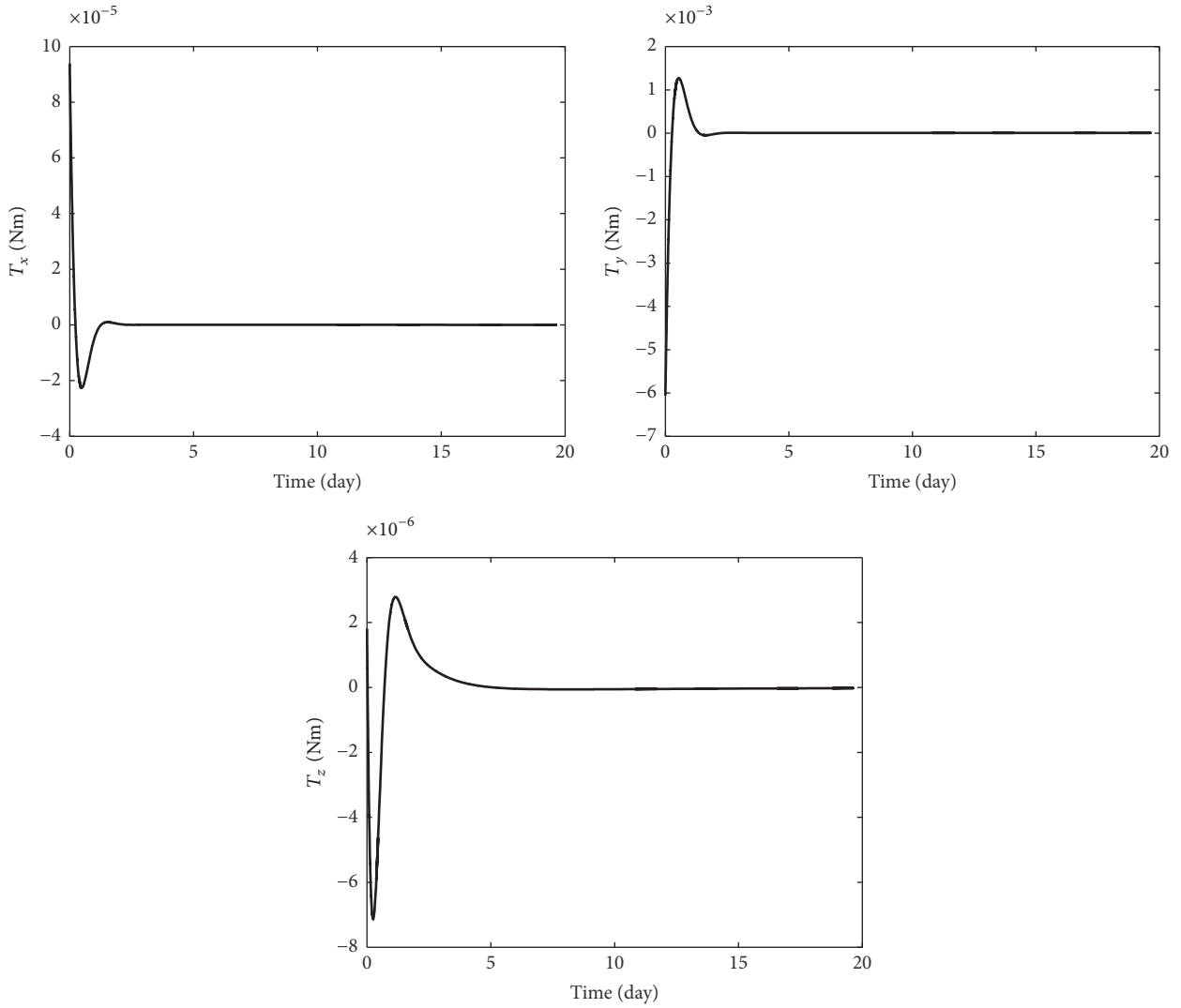

Figure 12: The control torques.

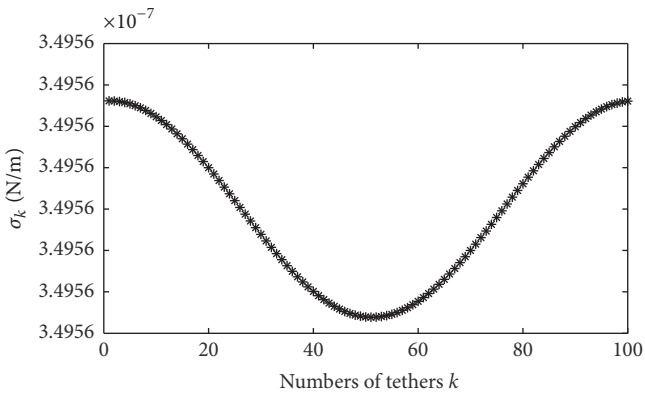

Figure 13: The thrust magnitudes per unit length of tethers at the beginning of the mission.

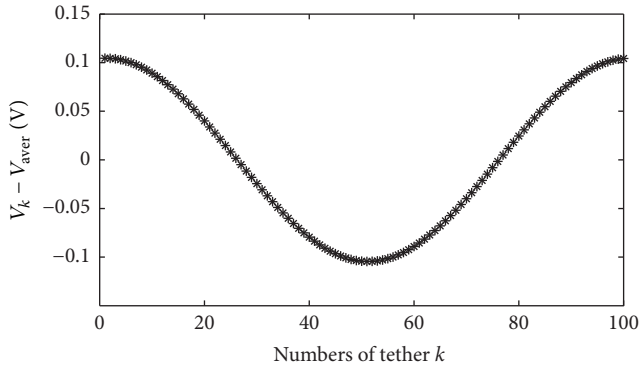

Figure 14: The voltage distribution of tethers at the beginning of the mission.

point of the coupled dynamical system in displaced orbit is obtained, and its stability is analyzed through a linearization. The results of stability analysis show that only some of the orbits are marginally stable. For unstable displaced orbits, linear quadratic regulator is employed to control the coupled orbit-attitude system. Numerical simulation shows that the linear quadratic regulator can control the coupled system and a small torque can stabilize both the attitude and orbit. To generate the control force and torque, the voltage distribution problem is converted into a nonlinear programming problem and solved using sequential quadratic programming in an optimal framework. The numerical results show that the control force and torque of electric sail can be realized by adjusting the voltage distribution of charged tethers.

Conflicts of Interest

The authors declare no competing financial interests.

Authors' Contributions

Mingying Huo and Yanfang Liu conceived and designed the experiments. Mingying Huo and He Liao performed the experiments and analyzed the data. Mingying Huo and Naiming Qi wrote the paper. All authors reviewed the manuscript.

Acknowledgments

This work was supported by Shanghai Academy of Spaceflight Technology (no. SAST2016039), the Open Fund of National Defense Key Discipline Laboratory of Micro-Spacecraft Technology (Grant no. HIT.KLOF.MST.201607), Heilongjiang Postdoctoral Foundation (no. LBH-Z16082), and China Postdoctoral Science Foundation (no. 2017M611372).

References

[1] P. Janhunen, P. Toivanen, J. Envall et al., "Overview of electric solar wind sail applications," *Proceedings of the Estonian Academy of Sciences*, vol. 63, no. 2S, pp. 267–278, 2014.

[2] C. R. McLnnes and J. F. L. Simmons, "Solar sail halo orbits I: heliocentric case," *Journal of Spacecraft and Rockets*, vol. 29, no. 4, pp. 466–471, 1992.

[3] C. R. McInnes, "Passive control of displaced solar sail orbits," *Journal of Guidance, Control, and Dynamics*, vol. 21, no. 6, pp. 975–982, 1998.

[4] C. R. McInnes, "Solar sail mission applications for non-keplerian orbits," *Acta Astronautica*, vol. 45, no. 4-9, pp. 567–575, 1999.

[5] S. Gong, H. Baoyin, and J. Li, "Coupled attitude-orbit dynamics and control for displaced solar orbits," *Acta Astronautica*, vol. 65, no. 5-6, pp. 730–737, 2009.

[6] S. Gong, J. Li, and H. Baoyin, "Analysis of displaced solar sail orbits with passive control," *Journal of Guidance, Control, and Dynamics*, vol. 31, no. 3, pp. 782–785, 2008.

[7] S. Gong, H. Baoyin, and J. Li, "Solar sail formation flying around displaced solar orbits," *Journal of Guidance, Control, and Dynamics*, vol. 30, no. 4, pp. 1148–1152, 2007.

[8] S. Gong, H. Baoyin, and J. Li, "Relative orbit design and control of formation around displaced solar orbits," *Aerospace Science and Technology*, vol. 12, pp. 195–201, 2008.

[9] J. Mu, S. Gong, and J. Li, "Coupled control of reflectivity modulated solar sail for GeoSail formation flying," *Journal of Guidance, Control, and Dynamics*, vol. 38, no. 4, pp. 740–751, 2015.

[10] S. Gong, J. Li, and H. Baoyin, "Formation flying solar-sail gravity tractors in displaced orbit for towing near-earth asteroids," *Celestial Mechanics & Dynamical Astronomy*, vol. 105, no. 1–3, pp. 159–177, 2009.

[11] J. Heiligers, C. R. McInnes, J. D. Biggs, and M. Ceriotti, "Displaced geostationary orbits using hybrid low-thrust propulsion," *Acta Astronautica*, vol. 71, pp. 51–67, 2012.

[12] P. Janhunen, "Electric sail for spacecraft propulsion," *Journal of Propulsion and Power*, vol. 20, no. 4, pp. 763-764, 2004.

[13] P. Janhunen, "Status report of the electric sail in 2009," *Acta Astronautica*, vol. 68, no. 5-6, pp. 567–570, 2011.

[14] G. Mengali and A. A. Quarta, "Non-Keplerian orbits for electric sails," *Celestial Mechanics and Dynamical Astronomy*, vol. 105, no. 1, pp. 179–195, 2009.

[15] N. Qi, M. Huo, and Q. Yuan, "Displaced electric sail orbits design and transition trajectory optimization," *Mathematical Problems in Engineering*, vol. 2014, Article ID 932190, 9 pages, 2014.

[16] M. Huo, J. Zhao, S. Xie, and N. Qi, "Coupled attitude-orbit dynamics and control for an electric sail in a heliocentric transfer mission," *PLoS ONE*, vol. 10, no. 5, article e0125901, 2015.

[17] P. K. Toivanen and P. Janhunen, "Spin plane control and thrust vectoring of electric solar wind sail," *Journal of Propulsion and Power*, vol. 29, no. 1, pp. 178–185, 2013.

[18] P. Janhunen, P. K. Toivanen, J. Polkko et al., "Electric solar wind sail: toward test missions," *Review of Scientific Instruments*, vol. 81, no. 11, article 111301, 2010.